

Performance evaluation of adaptive meshing algorithms for fluorescence diffuse optical tomography using experimental data

Lu Zhou,¹ Birsen Yazıcı,^{1,2,*} Angeliqe B. F. Ale,³ and Vasilis Ntziachristos³

¹Department of Electrical, Computer and Systems Engineering, Rensselaer Polytechnic Institute, 110 Eighth Street, Troy, New York 12180, USA

²Department of Biomedical Engineering, Rensselaer Polytechnic Institute, 110 Eighth Street, Troy, New York 12180, USA

³Institute for Biological and Medical Imaging (IBMI), Helmholtz Zentrum München, D-85764 Neuherberg, Germany

*Corresponding author: yazici@ecse.rpi.edu

Received May 4, 2010; revised September 23, 2010; accepted September 24, 2010;
posted October 7, 2010 (Doc. ID 127856); published November 2, 2010

Fluorescence diffuse optical tomography (FDOT) is a computationally demanding imaging problem. The discretizations of FDOT forward and inverse problems pose a trade-off between the accuracy and the computational efficiency of the image reconstruction. To address this trade-off, we analyzed the effect of discretization on the accuracy of FDOT imaging and proposed novel adaptive meshing algorithms for FDOT in a series of studies. In this Letter, we apply these new adaptive meshing algorithms to FDOT imaging using real data from a phantom experiment to demonstrate the practical advantages of our algorithms in FDOT image reconstruction. © 2010 Optical Society of America

OCIS codes: 170.6960, 170.3880, 170.3010.

Fluorescence diffuse optical tomography (FDOT) is an emerging imaging modality that can resolve the distribution of fluorescent probe in tissue, thereby providing a way to visualize and quantify specific molecular targets, pathways, and physiological effects *in vivo* [1]. Because of the diffusive nature of light propagation in tissue, FDOT is an intrinsically three-dimensional and computationally demanding nonlinear imaging problem that involves repeated solutions of the forward and inverse problems. Given N_S sources and N_D detectors, the FDOT inverse problem involves recovering the unknown fluorophore concentration μ in a domain Ω from the measurements obtained on the domain boundary $\partial\Omega$ based on the following integral equation [2]:

$$\Gamma_{ij} = \int_{\Omega} g_j^*(\mathbf{r}) \phi_i(\mathbf{r}) \mu(\mathbf{r}) d\mathbf{r},$$

where $\mathbf{r} \in \Omega$, Γ_{ij} is the emission light field measured by the j th detector, $j = 1, \dots, N_D$, due to the i th source, $i = 1, \dots, N_S$, ϕ_i is the excitation field generated by the i th source, and g_j^* is the Green's function of the diffusion equation that models the emission light propagation due to a point source located at the j th detector position. Clearly, solving the inverse problem requires first solving for ϕ_i and g_j^* based on the diffusion model for each source-detector pair, which defines the FDOT forward problem.

For an arbitrary domain geometry and nonhomogeneous background optical properties, both problems need to be discretized and solved numerically. The numerical solutions pose a trade-off between the accuracy and the computational efficiency of image reconstruction. To address this trade-off, adaptive discretization techniques have been developed for FDOT imaging to improve the reconstruction accuracy while reducing the computational requirements [2–6]. In a series of papers, we first analyzed the effect of discretization on the

accuracy of FDOT imaging and proposed novel adaptive meshing algorithms under the assumption that the measurements are noise free [2,5]. In [6], we extended our work to the case of noisy measurement and took into account noise statistics in designing adaptive meshes. In this Letter, we evaluate the performance of the adaptive meshing algorithms developed in [6] using real data obtained from a phantom experiment and demonstrate the practical advantages of our algorithms in FDOT imaging:

$$\varepsilon_f^i(k) := \sum_{j=1}^{N_D} \frac{1}{\sigma_{ij}^2} \left[\|g_j^* \phi_i\|_0 \left[\|g_j^* \mu\|_{0,ni} + \sum_{i',j'}^{N_S, N_D} \|g_j^* D_{i'j'} \pi_{i'j'}\|_{0,ni} \right] + [|\Gamma_{ij}| + D_{ij}] \|g_j^*\|_{\infty,ni} \right] \cdot \|\phi_i\|_{1,ni} h_{ni}, \quad (1)$$

$$\varepsilon_f^j(k) := \sum_{i=1}^{N_S} \frac{1}{\sigma_{ij}^2} \left[\|g_j^* \phi_i\|_0 \left[\|\phi_i \mu\|_{0,mj} + \sum_{i',j'}^{N_S, N_D} \|\phi_i D_{i'j'} \pi_{i'j'}\|_{0,mj} \right] + [|\Gamma_{ij}| + D_{ij}] \|\phi_i\|_{\infty,mj} \right] \cdot \|g_j^*\|_{1,mj} h_{mj}, \quad (2)$$

$$\varepsilon_i(k) := \left[\sum_{i,j}^{N_S, N_D} \frac{\|G_j^* \Phi_i\|_0}{\sigma_{ij}^2} \|G_j^* \Phi_i\|_{0,t} + \frac{1}{\kappa} \|\infty,t\| \right] \times \left[\|\mu\|_{1,t} + \sum_{i,j}^{N_S, N_D} \|D_{ij} \pi_{ij}\|_{1,t} \right] h_t. \quad (3)$$

For both FDOT forward and inverse problems, the adaptive meshing algorithms, developed in [6], are initiated with coarse uniform meshes. At each refinement iteration, an error indicator for each element of the mesh as well as their average values are computed. Then, the element with error indicator value greater than the

average is refined until the total number of nodes in the mesh exceeds a predetermined limit. In a mesh with N elements for the forward problem solutions ϕ_i or g_j^* , or the inverse problem solution μ , the error indicators for the k th element, $k = 1, \dots, N$, are given in Eqs. (1)–(3), respectively [6,7].

In the phantom experiment, we used a cylindrical phantom made of silicone rubber with 2 cm diameter and 4 cm height, as shown in Fig. 1(a). The phantom had homogeneous absorption coefficient $\mu_a = 0.2 \text{ cm}^{-1}$ and reduced scattering coefficient $\mu'_s = 12 \text{ cm}^{-1}$ at both 743 and 767 nm wavelengths. The phantom contained a hollow tube with 3 mm diameter along the central axis. The tube was filled with $1 \mu\text{M}$ Cy7 (excitation at 743 nm, emission at 767 nm) mixed with intralipid and ink to mimic the same background optical properties of the phantom base.

The optical measurements were collected using the FDOT imaging system reported in [8], as illustrated in Fig. 1(b). Specifically, a focused collimated laser beam was used as a source on one side of the phantom at 24 different positions sequentially (on a 3×8 grid, over a $10 \text{ mm} \times 15 \text{ mm}$ field of view). On the other side of the phantom, an electrically cooled CCD camera was placed to collect the cw fluorescence measurements for each source position. In the image obtained by the CCD camera, we selected 36 subimages, each with 6×6 pixels (on a 4×9 grid, over a $10 \text{ mm} \times 20 \text{ mm}$ field of view) on the phantom as the virtual detectors, and the reading of each detector was calculated as the mean pixel value of each subimage. After collecting a set of measurements for all 24 source positions, the phantom was rotated by 180° to obtain another set of measurements.

In the image reconstruction, we formulate the FDOT inverse problem as the maximum *a posteriori* estimator of the fluorophore concentration with a noise model in which the noise variance is proportional to the magnitude of the measurements [6]. We empirically chose the regularization parameter and kept it the same for different meshing schemes. We used both uniform and adaptive meshes generated by our algorithms with hexahedral finite elements and trilinear Lagrange basis functions to discretize the forward and inverse problems on the cylindrical domain Ω . The mesh refinement and image reconstruction were performed on a computer with 3.4 GHz dual-core CPU and 2 GB memory, and

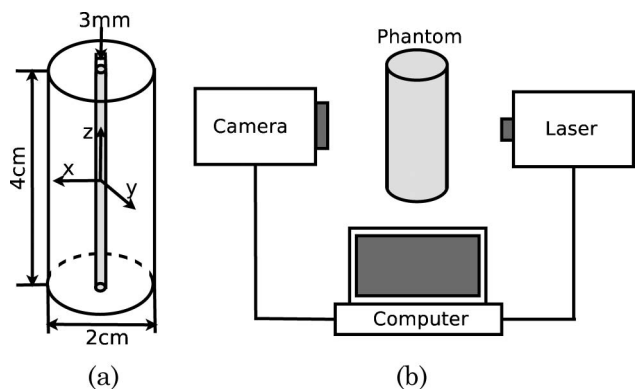


Fig. 1. (a) Phantom used in the experiment. (b) FDOT imaging system setup.

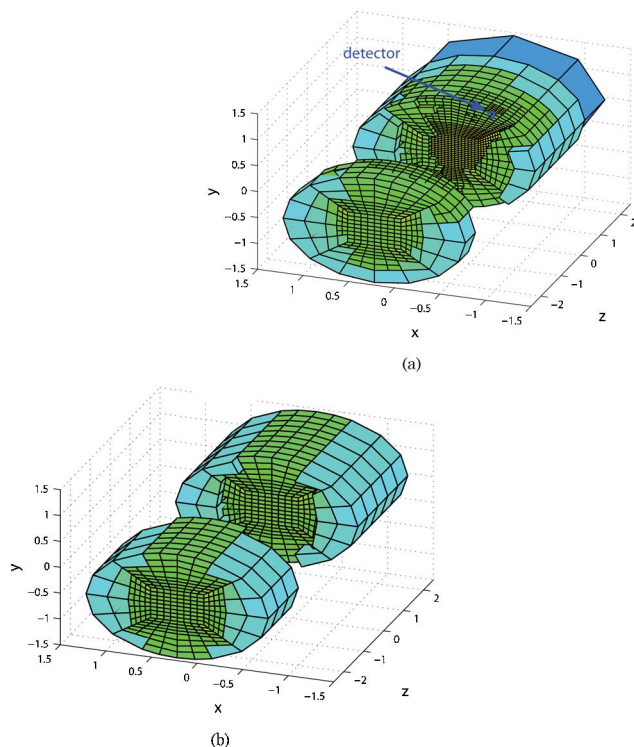


Fig. 2. (Color online) Adaptive mesh generated by our algorithm for (a) the detector at $(-0.47, 0.88, -1.12)$, (b) the inverse problem.

the reconstruction time including mesh refinement for each image was approximately 5–10 min.

Figure 2 shows the adaptive meshes generated by our algorithms. For the detector at position $(-0.47, 0.88, -1.12)$, our algorithm generated its mesh with higher resolution not only around that detector but also around the fluorophore heterogeneity and some sources close to the detector. For the inverse problem, our algorithm generated the mesh with higher resolution around the fluorophore heterogeneity, as well as source and detector positions. Figure 3 shows the relationship between the average number of nodes in the adaptive mesh for a certain source or detector and the z coordinate of its position. We observed that our algorithm generated finer meshes for the sources and detectors toward the center of the source and detector grids. We also observed that the measurements on these sources and detectors had higher magnitude, indicating higher signal-to-noise

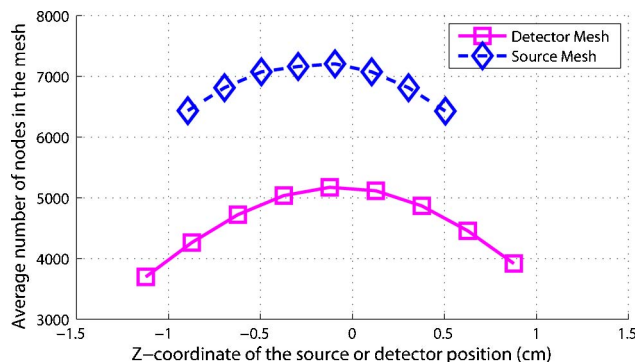


Fig. 3. (Color online) Relationship between the average number of nodes in the forward adaptive mesh for a certain source or detector and the z coordinate of its position.

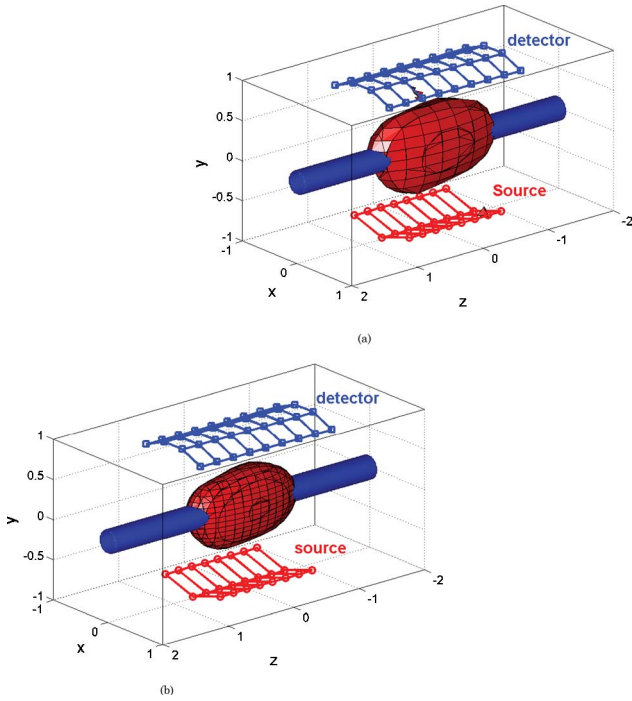


Fig. 4. (Color online) Fluorophore heterogeneity reconstructed using (a) uniform meshes and (b) the adaptive meshes. The blue tube indicates the true fluorophore heterogeneity.

ratio (SNR) for these measurements. This result is consistent with our numerical simulation in [6], which indicates that our algorithms generate the forward adaptive meshes with varying resolutions for different source-detector pairs depending on the SNR of the associated measurements.

Figure 4 shows the reconstructed surface of the fluorophore heterogeneity with the concentration value equal to the half of the maximum value reconstructed in the image. We observe that the image in Fig. 4(b) reconstructed by using our adaptive meshing algorithms has a shape closer to the true tube-shaped fluorophore heterogeneity than the image reconstructed by uniform meshes shown in Fig. 4(a).

To quantitatively assess the reconstruction accuracy, we discretized the domain using a fine uniform mesh with 91,377 nodes to obtain a baseline image with negligible error due to discretization and calculated the $L^2(\Omega)$ -norm of the error in the images reconstructed using the coarse uniform and adaptive meshes. Note that the image reconstruction time on this fine mesh is approximately 40–50 min. We also calculated the maximum width along the x direction of the reconstructed fluorophore heterogeneities, as well as the volume outside the fluorophore heterogeneity for images shown in Fig. 4 to quantify the

Table 1. Discretization Error, Maximum Width Along x Direction, and the Volume outside the Fluorophore Heterogeneity Reconstructed by Using Different Meshes

	Discretization Error	Maximum Width	Volume Outside
Uniform	6.096×10^{-3}	5.273 mm	8.342 cm ³
Adaptive	3.283×10^{-3}	4.395 mm	9.131 cm ³

resolution. The results, summarized in Table 1, indicate the improvements in the reconstruction accuracy as well as the image resolution due to adaptive meshing algorithms.

In this Letter, we demonstrated the advantages of the adaptive meshing algorithms developed in [6] using measurements collected in a phantom experiment. In FDOT image reconstruction, the measurement noise is an important factor that affects the reconstruction accuracy. We showed that the adaptive meshing algorithms that take into account noise statistics can effectively improve the accuracy and resolution of the FDOT image reconstruction as compared to the uniform meshing scheme for a given fixed number of nodes.

This work was supported by U. S. Army Medical Research-W81XWH-04-1-0559 and by the Center for Sub-surface Sensing and Imaging Systems, under the Engineering Research Centers Program of the National Science Foundation (NSF) (award EEC-9986821).

References and Notes

1. R. Weissleder and V. Ntziachristos, *Nat. Med.* **9**, 123 (2003).
2. M. Guven, L. Reilly-Raska, L. Zhou, and B. Yazici, *IEEE Trans. Med. Imaging* **29**, 217 (2010).
3. W. Bangerth and A. Joshi, *Inverse Probl.* **24**, 034011 (2008).
4. J. Lee, A. Joshi, and E. Sevick-Muraca, *Opt. Express* **15**, 6955 (2007).
5. M. Guven, L. Zhou, L. Reilly-Raska, and B. Yazici, *IEEE Trans. Med. Imaging* **29**, 230 (2010).
6. L. Zhou and B. Yazici, "Discretization error analysis and adaptive meshing algorithms for fluorescence diffuse optical tomography in the presence of measurement noise," *IEEE Trans. Image Process.* (to be published).
7. In Eqs. (1)–(3), $D_{ij} = [\sigma_{ij}^2 + \int_{\Omega} \kappa(\mathbf{r}) \phi_i^2(\mathbf{r}) (g_j^*)^2(\mathbf{r}) d\mathbf{r}]^{1/2}$, where σ_{ij}^2 is the noise variance in Γ_{ij} , κ represents the variance of μ , π_{ij} is the inverse problem solution when $\Gamma_{ij} = 1$ and $\Gamma_{kl} = 0$, for all $kl \neq ij$, $k = 1, \dots, N_S$ and $l = 1, \dots, N_D$. Note that we use $\|\cdot\|_{\infty,k}$, $\|\cdot\|_{0,k}$, and $\|\cdot\|_{1,k}$ to denote the L^∞ , L^2 , and H^1 norms of a function on the k th element, and use $\|\cdot\|_{\infty}$ and $\|\cdot\|_0$ to denote the L^∞ and L^2 norms of a function on the domain Ω .
8. N. Deliolanis, T. Lasser, D. Hyde, A. Soubret, J. Ripoll, and V. Ntziachristos, *Opt. Lett.* **32**, 382 (2007).